CHAPTER IV
PREPARATION OF MESOPOROUS CeO_2-ZrO_2 FOR CATALYTIC CONVERTER

4.1 Abstract

Currently, there is a great amount of ongoing research involved in catalytic converters because of their interesting applications in eliminating toxic gases from exhaust pipes. Many types of porous materials have been widely studied and used to increase the catalytic activity. In this work, mesoporous ceria-zirconia (CeO_2-ZrO_2) was synthesized using MCM-48 as a hard template via the nanocasting method. The obtained product provided a high surface area of 248.5 m^2/g. The optimum conditions were to stir for 4 h at 100 °C evaporation temperature of solvent. The synthesized mesoporous CeO_2-ZrO_2 was characterized using X-ray diffraction (XRD), X-ray fluorescence (XRF), Transmission electron microscopy (TEM), and N_2 adsorption/desorption. The Temperature-programmed reduction results provided only surface reduction temperatures at 280-620 °C.

Keywords: Ceria-Zirconia, Mesoporous, Nanocasting method

4.2 Introduction

Porous materials have been widely studied because of their remarkable properties, such as high surface areas, which is attractive in many applications, especially catalyst supports. According to the IUPAC definition, it can be divided into three categories relied on their pore sizes, viz. microporous (pore size <2 nm), mesoporous (2-50 nm), and macroporous (>50 nm) [1]. Mesoporous materials are more preferred for its highly ordered mesostructure, high surface area, and larger pore size than microporous materials, thus allowing diffusion and adsorption of higher molecular weight molecules [2]. The porous structure with uniform mesopore can increase the surface-to-volume ratio and the surface area of materials [3].

Cerium oxide (CeO_2) is one of rare earth metal oxide extensively employed for various applications, especially for automotive exhaust catalyst, because it has a redox properties of Ce^{3+}/Ce^{4+}, which provides high catalytic activities, and ability to storage or release oxygen between CeO_2 and Ce_2O_3 [4-5]. Thus, CeO_2 is used for automotive exhaust gas treatment, as a three-way catalyst (TWCs) [5] to convert the hydrocarbon (HCs), CO, and NO_x presenting in the automotive exhaust to H_2O, CO_2, and N_2 [6].

Zirconium oxide (ZrO_2) is the only metal oxide that has acidity and basicity properties as well as reducing and oxidizing abilities. ZrO_2 has at least three crystalline transformation; cubic, tetragonal, and monoclinic [7-8]. Excellent properties of zirconia are mechanical resistance, chemical stability, and redox properties [9].

Mesoporous ceria-zirconia oxide with high surface area is synthesized by nanocasting method using either soft or hard templates. Use of a hard template can control the final properties of the catalyst structure after the removal of the template, leading to well-ordered structure of nanostructured mesoporous material [10-11].

In this research, the objective was to prepare the mesoporous CeO_2-ZrO_2 via nanocasting method using MCM-48 as a hard template, synthesized from silatrane, as silica precursor and introduced by Wongkasemjit's research group [12-13]. The optimal conditions to obtain high surface area and CeO_2-ZrO_2 single phase were investigated.

4.3 Experimental

4.3.1 Materials

Fumed silica (SiO_2, 99.8%, Nippon Aerosil, Japan), UHP grade nitrogen (N_2, 99.99% purity, Thai Industrial Gases Public Company Limited (TIG), Thailand), ethylene glycol (EG, 99%, J.T. Baker, USA), TEA (QRëc chemical, Thailand), acetonitrile (CH_3CN, 99.9%, Labscan, Thailand), ethanol (CH_3CH_2OH, 99.9%, Labscan, Thailand), cetryltrimethylammonium bromide ($C_{19}H_{42}BrN$, 99.9%, Fluka Analytical), sodium hydroxide (NaOH, 99%, Labscan, Thailand), ceriumnitrate hexahydrate ($Ce(NO_3)_3.6H_2O$, 99%, Aldrich), zirconium oxide chloride octahydrate ($ZrOCl_2.8H_2O$, 99.9%, Merck) were directly employed with no further purification.

4.3.2 Synthesis Method

4.3.2.1 Synthesis of Silatrane

The synthetic method was followed Wongkasemjit's method by mixing 0.1 mol fumed silica, 100 ml EG, and 0.125 mol TEA [12]. The mixture was refluxed at 200 °C under nitrogen atmosphere for 10 h in an oil bath. The excess EG was removed under vacuum at 110 °C. The white silatrane product was washed with acetronitrile to remove excess TEA and EG. The white silatrane product was vacuum-dried overnight before characterization using TGA and FT-IR.

4.3.2.2 Synthesis of Mesoporous MCM-48

The synthesis of mesoporous MCM-48 was followed Wongkasemjit's synthetic method by using 2M NaOH to dissolve and CTAB, as surfactant, at 50 °C [13]. Silatrane was then added to the mixture solution and stirred the mixture for 1 h. The molar composition ratio of the mixture was $0.3CTAB:0.5NaOH:62H_2O:1.0SiO_2$. The mixture was treated at 140 °C for 16 h in a Teflon-lined stainless steel autoclave to obtain solid product. The white solid product was collected by filtration and dried at ambient conditions. The surfactant was removed by calcinations at 550 °C for 6 h with a heating rate of 0.5 °C/min to obtain

MCM-48. The obtained white product, MCM-48, was characterized by FE-SEM and XRD.

4.3.2.3 Synthesis of Mesoporous Ceria-Zirconia

The synthesis of mesoporous ceria-zirconia was followed Wongkasemjit's synthetic method [14] by mixing cerium nitrate and zirconium oxide chloride with various ratios (100:0, 75:25, and 60:40 mol%) and MCM-48 as silica hard template in ethanol. After stirring for various times (30 min, 1, 2, and 4 h), ethanol in the mixture was removed by evaporation in an oven set at different temperatures (ambient temperature, 50 °C, 100 °C). The obtained powder is heated in a ceramic crucible at 550 °C for 6 h to decompose the nitrate and chloride species. Removal of the hard template was carried out using 2M NaOH at 50 °C for 3 times and the mixture was centrifuged to obtain the product. The product was washed by deionized water and centrifuged until it was neutral and dried at 100 °C. The obtained products were characterized by FE-SEM, TEM, XRD, XRF, and N_2 adsorption/desorption.

4.3.3 Materials Characterization

X-ray diffractrometer (XRD) was used to identify the crystalline phases present in the structure. The diffraction pattern was the fingerprint of any crystalline phase. The phase of mesoporous products was characterized on a Rigaku DMAX 2200HV XRD with a scanning speed of 1 °C/min and CuKα source (λ= 0.154 Å) in a range of 2θ = 2–6°. Transmission electron microscope (TEM, JEOL JEM-2010) was used to provide further exploration in morphology and structure, including dimension of samples. Temperature programmed reduction (TPR, Thermofinnigan) with hydrogen was performed in a flow reaction system using 9.6 % hydrogen in argon used as a carrier gas (flow rate: 18.3 ml/min). The ordered mesoporous ceria, mesoporous bimetallic ceria-zirconia (0.10 g) were heated from room temperature to 900 °C with a linear ramp rate of 5 °C/min. Field emission scanning electron microscope (FE-SEM, Hitachi FE-SEM TM-3000) was used to determine the size, morphology, and the pore system of particles. Thermogravimetric analyzer (TGA, Perkin-Elmer) was used to analysis thermal properties by measuring the change in mass of solid material as a function of temperature or time. N_2

adsorption/desorption measurement was used to determine into the pore structure of porous material, such as the inner pore surface area, the pore volume and the pore diameter distribution. Fourier transforms infrared spectrophotometer (FT-IR, Nicolet) was used to investigate the functional groups of chemical composition. X-ray fluorescence spectrophotometer (XRF, AXIOS PW 4400) was used to analyze the metal contents in samples.

4.4 Results and Discussion

The synthesis of mesoporous (MSP) ceria-zirconia via nanocasting process is followed Wongkasemjit's synthetic method [14] by using 50 % wt of MCM-48 mixed with zirconium and cerium precursors. The molar ratio of ceria-zirconia was fixed at 0.75 mol ceria and 0.25 mol zirconia.

4.4.1 Nanocasting Process

4.4.1.1 Effect of Stirring Time

The effect of stirring time (30 min, 1, 2, and 4 h) of the precursors and the template in solvent was studied using 0.75 mol of ceria and 0.25 mol of zirconia. Figure 4.1 shows the small angle XRD pattern of MCM-48 and ceria-zirconia at various stirring times. The XRD pattern of MCM-48 (Fig. 4.1a) shows reflection peaks at {211}, {220}, {420}, and {332} corresponding to the *Ia3d* cubic structure [13]. However, the results from the mixture (Fig. 4.1b) reveal characteristic peaks only at {211} and {220}, similar to the work reported by Abdollahzadeh-Ghom and co-workers [15], who synthesized ceria-zirconia MSP material using SBA-15 and KIT-6 respectively, as a hard template. For the replicas, the main reflection is slightly shifted to a smaller angle, probably referring to a bigger pore size than the template pores [15]. These results could be concluded that all replica still maintained some order from their template.

N_2 adsorption-desorption isotherms and pore size distribution of the synthesized ceria-zirconia are shown in Fig. 4.2. All isotherms show an obvious uptake of N_2 as a result of capillary condensation in wide relative pressure (P/P_0) range of 0.55-0.99, indicating the existence of multiform pore distributions.

The pore size distribution in Fig. 4.2b was calculated from the desorption branch of the isotherms using BJH method. As can be seen, they possessed bimodal pore size distributions in the MSP range of 2-50 nm. These pores are larger than the wall thickness of MCM-48 (1.53 nm) and ascribe to the coalescence of unfilled spaces of the MCM-48 template or/and the voids between the small particles [16]. Thus, it can be stated that the obtained product was indeed MSP with high BET surface area.

Surface areas of all synthesized MSP ceria-zirconia are summarized in Table 4.1. The 4 h stirring time provided the highest surface area and more uniform pore size (Fig 4.2b), leading to higher order. Thus, the suitable condition of the stirring time is at 4 h.

4.4.1.2 Effect of Evaporated Temperature

The evaporated temperature of solvent also affects the MSP synthesis because the metal precursors adhere with a MSP silica template and were anticipated to move and impregnate into the pore during the evaporation of solvent [17]. Another word, the evaporated temperature influences on how fast the precursors migrate or penetrate. Ethanol was chosen as a solvent in this process because of its solubility and low boiling point around 78 °C, easy to evaporate [1]. The temperatures studied were at ambient, 50°, and 100 °C. Figure 4.3 shows the small angle XRD patterns of the MSP ceria-zirconia fabricated at the studied temperatures. All replicas provided the diffraction peak at {211} and {220} even though the intensity from each temperature was different. At the ambient temperature the XRD pattern of the product was less order than the others, but still retained some order of the original MSP structure. Thus, it can be summarized that the structure of MCM-48 still maintained although the higher temperature resulted in the more order of the product.

Surface area results of those three evaporated samples are in agreement with the XRD results and listed in Table 4.2. At 100 °C evaporated temperature the product provided the highest surface area (248.5 m^2/g) probably due to the shortest time to evaporate solvent (around 1–1.30 h). Comparing to the ambient and 50 °C evaporated temperatures, the process took longer time to evaporate, 2 days and 12 h, respectively, making more precursors to migrate inside

the pore, blocking the pores, and distorting the structure [18]. Thus, the appropriate evaporated temperature in this study was at 100 °C.

SEM and TEM images of MSP $Ce_{0.75}Zr_{0.25}O_2$ at 4 h stirring time and 100 °C evaporated temperature are shown in Fig. 4.4. The SEM image (Fig. 4.4a) has a very small spherical morphology while the TEM image in Fig. 4.4b confirms the MSP structure of the sample, similar to the MSP template structure.

4.4.1.3 Effect of Ceria-Zirconia Molar Ratio

The effect of ceria-zirconia molar ratio was studied because the addition of zirconia to ceria can enhance the thermal stability of ceria. The MSP $Ce_{1-x}Zr_xO_2$ where x = 0.25 ($Ce_{0.75}Zr_{0.25}O_2$) and 0.40 ($Ce_{0.60}Zr_{0.40}O_2$) were synthesized using the optimal conditions of 4 h stirring time and 100 °C evaporated temperature.

The small angle XRD patterns of samples with different content of ceria and zirconia are shown in Fig. 4.5. The XRD results also show the diffraction peak at {211} and {220}, referring to the structure of MCM-48, meaning that the order structure of template still retained.

To confirm the crystallinity of MSP ceria and ceria-zirconia, wide angle XRD was used to analyze, as shown in Fig. 4.6. The XRD pattern of MSP ceria (Fig 4.6a) shows peaks at 2θ = 29°, 33.2°, 47.2°, 56.3°, 59.1°, 69.3°, 76.8°, and 78.9°, corresponding to the plane reflections of {111}, {200}, {220}, {311}, {222}, {400}, and {311}, respectively. The peak pattern is belonging to the cubic fluorite structure [11]. Comparing the XRD patterns among them, it is seen that the MSP $Ce_{0.75}Zr_{0.25}O_2$ pattern (Fig. 4.6b) is similar to the MSP CeO_2 pattern (Fig 4.6a) while there was some tetragonal phase of the zirconia in the prepared $Ce_{0.60}Zr_{0.40}O_2$ XRD pattern (Fig. 4.6c) at 2θ = 30°, 50°, and 60°, corresponding to the {111}, {220}, and {222} reflections, respectively. The results suggest that the MSP $Ce_{1-x}Zr_xO_2$ preferably crystallizes into a cubic fluorite structure if x is equal to or lower than 0.25 as reported by Thammachart and co-workers [19]. The presence of only the cubic phase means that ceria and zirconia are highly, homogeneously distributed [19]. Furthermore, the XRD peak of silica at 2θ = 22° was not detected, indicating that the silica template could be completely removed [20].

The presence of the silica template was also analyzed by XRF technique and the results are listed in Table 4.3, showing that after removing the silica template from the MSP $Ce_{1-x}Zr_xO_2$, there was small amount of silica still remained. The found contents of Ce and Zr were lower than the loaded values, probably due to the loss of Ce and Zr precursor in the basic medium during the nanocasting process [21].

Surface areas of MSP $Ce_{1-x}Zr_xO_2$ are listed in Table 4.4. As seen from the table, the specific surface area decreased when increasing the zirconia content because when the zirconia precursor was dissolved in the solvent, it forms $[Zr_4(OH)_8(H_2O)_{16}]^{8+}$. Depending on the concentration, further hydrolysis of the tetramer lead to either oligomers or crystal nuclei, probably less infiltrated into the pore [22]. This is in agreement with wide angle XRD results in Fig. 4.6 which indicates the tetragonal phase of zirconia. As a result, addition of higher content of zirconia distorted the structure and decreased the surface area.

4.4.2 Temperature Programmed Reduction (TPR)

The reduction property of the nanocasting ceria-zirconia was investigated in order to observe the H_2 consumption of the sample using TPR technique. The TPR profiles as a function of the temperature of the order MSP $Ce_{0.60}Zr_{0.40}O_2$, $Ce_{0.75}Zr_{0.25}O_2$, and CeO_2 are shown in Fig. 4.7. The TPR profile of MSP CeO_2 (Fig. 4.7a) provided the first peak at a low temperature range of 280°–600 °C, corresponding to the surface reduction while the second peak at 680°–820 °C is referred to the reduction of the bulk phase lattice oxygen. A higher thermal condition to reduce Ce^{4+} to $Ce^{3+}$is required for the reduction of the bulk phase lattice oxygen [23]. The TPR profile of MSP $Ce_{0.75}Zr_{0.25}O_2$ (Fig. 4.7b) was similar to that of the MSP CeO_2, except the lower intensity, meaning that the reduction of the bulk phase lattice oxygen is very small [24]. Like-wise, the TPR profile of MSP $Ce_{0.60}Zr_{0.40}O_2$ (Fig. 4.7c) gave two peaks at 350° to 700 °C and 750° to 850 °C.

It is difficult to separate the reduction of each species, ceria or zirconia, and their relative amounts of H_2 consumed in the TPR profiles of MSP ceria-zirconia due to the width of the peaks and their overlapping [25]. However, adding more zirconia content tended to widen the reduction temperature range and

decrease the bulk phase lattice oxygen. The area under the peak is related to the H_2 consumption of the sample, meaning that the higher H_2 consumption provides the higher surface area which in agreement with the TPR profiles of this study.

4.5 Conclusions

The order MSP ceria-zirconia was successfully synthesized using MSP MCM-48 as a hard template via the nanocasting process. The optimal conditions studied were to use 4 h stirring time at 100 °C evaporated temperature. The XRD and TEM results confirmed the existence of the order MSP structure from the MCM-48 template whereas the XRF results confirmed the removal of the silica template from the order MSP ceria-zirconia. Comparing the molar ratio of ceria-zirconia; the MSP $Ce_{0.75}Zr_{0.25}O_2$ exhibited higher surface area and more homogenous distribution than the MSP $Ce_{0.60}Zr_{0.40}O_2$. The resulting product provided similar pattern to cubic fluorite structure of ceria. The TPR profiles had a wide range reduction temperature and resulted in a decrease in the bulk phase lattice oxygen when adding the zirconia content. The TPR results of the MSP $Ce_{0.75}Zr_{0.25}O_2$ provided only surface reduction temperatures at 280–620 °C.

4.6 Acknowledgements

This work is supported by the Petroleum and Petrochemical College and the Excellent Center for Petrochemical and Materials Technology, Ratchadapisake Sompote, Chulalongkorn University.

4.7 References

1. Lu, A-H., Zhao, D., and Wan, Y. (2009) Nanocasting: A Versatile Strategy for Creating Nanostructured Porous Materials. (pp.1-28) London: The Royal Society of Chemistry.
2. Angevine, P.J., Gaffney, A.M., Shan, Z., Koegler, J.H., Yeh, C.Y. "TUD-1: A generalized mesoporous catalyst family for industrial applications." Digital Refining. Dec 2008. 10 May 2013 <www.digitalrefining.com/article/1000209>.
3. Ma, X., Feng, X., He, X., Guo, H., Lv, L., Guo, J., Cao, H., and Zhou, T. (2012) Mesoporous CuO/CeO_2 bimetal oxides: One-pot synthesis, characterization and their application in catalytic destruction of 1,2-dichlorobenzene. Microporus and Mesoporous Materials, 158, 214-218.
4. Ji, P., Zhang, J., Chen, F., and Anpo, M. (2008) Ordered mesoporous CeO_2 synthesized by nanocasting from cubic Ia3d mesoporous MCM-48 silica: formation, characterization and photocatalytic activity. Journal of Physical Chemistry C, 112, 17809-17813.
5. Shen, W., Dong, X., Zhu, Y., Chen, H., and Shi, J. (2005) Mesoporous CeO_2 and CUO-loaded mesoporous CeO_2: Synthesis, characterization, and CO catalytic oxidation property. Microporous and Mesoporous Materials, 85, 157-162.
6. Kaspar, J., Fornasiero, P., and Graziani, M. (1999) Use of CeO_2-based oxides in the three-way catalysis. Catalysis Today, 50, 285-298.
7. Kuo, C.-W., Shen, Y.-H., Wen, S.-B., Lee, H.-E., Hung, I.M., Huang, H.-H. and Wang, M.-C. (2011) Phase transformation kinetics of 3 mol% yttria partially stabilized zirconia (3Y-PSZ) nanopowders prepared by a non-isothermal process. Ceramics International, 37(1), 341-347.
8. Wang, C.-H., Wang, M.-C., Du, J.-K., Sie, Y.-Y., Hsi, C.-S. and Lee, H.-E. (2013) Phase transformation and nanocrystallite growth behavior of 2 mol% yttria-partially stabilized zirconia (2Y-PSZ) powders. Ceramics International, 39(5), 5165-5174.

9. Ballem, A.M., Cordoba, M.J., and Oden, M. (2011) Mesoporous silica template zirconia nanoparticles. Journal of Nanoparticle Research, 13, 2743-2748.
10. Kong, A., Zhu, H., Wang, W., Zhang, Q., Yang, F., and Shan, Y. (2011) Novel nanocasting method for synthesis of ordered mesoporous metal oxides. Journal of Porous Materials, 18, 107-112.
11. Aranda, A., Solsana, B., and Garcia, T. (2010) Total oxidation of naphthalene using mesoporous CeO_2 catalysts synthesized by nanocasting from two dimensional SBA-15 and three dimensional KIT-6 and MCM-48 silica templates. Catalysis Letters, 134, 110-117.
12. Charoenpinijkarn, W., Suwankruhasn, M., Kesapabutr, B., Wongkasemjit, S., and Jamieson, A. (2001) Sol-gel processing of silatranes. European Polymer Journal, 37, 1441-1448.
13. Longloilert, R., Chaisuwan, T., Luengnaruemitchai, A., and Wongkasemjit, S. (2011) Synthesis of MCM-48 from silatrane via sol-gel process. Journal of Sol-Gel Science and Technology, 58, 427-435.
14. Deeprasertkul, C., Longloilert, R., Chaisuwan, T., and Wongkasemjit, S. (2014) Impressive low reduction temperature of synthesized mesoporous ceria via nanocasting. Materials Letters, 130, 218-222.
15. Abdollahzadeh-Ghom, S., Zamani, C., Andreu, T., Epifani, M. and Morante, J.R. (2011) Improvement of oxygen storage capacity using mesoporous ceria–zirconia solid solutions. Applied Catalysis B: Environmental, 108–109(0), 32-38.
16. Wang, Y., Li, B., Zhang, C., Cui, L., Kang, S., Li, X., and Zhou, L. (2013) Ordered mesoporous CeO_2-TiO_2 composites: Highly efficient photocatalysts for the reduction of CO_2 with H_2O under simulated solar irradiation. Applied Catalysis B: Environmental, 130-131, 277-284.
17. Yue, W., and Zhou, W. (2008) Crystalline mesoporous metal oxide. Progress in Natural Science, 18, 1329-1338.
18. Horikawa, T., Do, D. D., and Nicholson, D. (2011) Capillary condensation of adsorbates in porous materials. Advances in Colloid and Interface Science, 169, 40-58.

19. Thammachart, M., Meeyoo, V., Risksomboon, T., and Osuwan, S. (2001) Catalytic activity of CeO_2-ZrO_2 mixed oxide catalysts prepared via sol-gel technique: CO oxidation. Catalysis Today, 68, 53-61.
20. Roggenbuck, J., Schafer, H., Tsoncheva, T., and Tiemann, M. (2007) Mesoporous CeO_2: synthesis by nanocasting, characterization and catalytic properties. Microporous and Mesoporous Materials, 101, 335-341.
21. Maneesuwan, H., Tantisriyanurak, S., Chaisuwan, T., and Wongkasemjit, S. (2014) Impressivephenol hydroxylation activity using Fe-Ti-TUD-1 synthesized from silatrane via sol-gel process. Applied Catalysis A: General (in press).
22. Chen, K. L., Chiang Anthony, S. T., and Tsao, H. K. (2001) Preparation of zirconia nanocrystals from concentrated zirconium aqueous solutions. Journal of Nanoparticle Research, 3, 119-126.
23. Rao, R. G., Sahu, R., and Mishra G. B. (2003) Surface and catalytic properties of Cu-Ce-O prepared by combustion method. Colloids and Surfaces A: Physicochemical and Engineering, 220, 261-269.
24. Zhu, H., Qin, Z., Shan, W., Shen, W., and Wang, J. (2004) Pd/CeO_2–TiO_2 catalyst for CO oxidation at low temperature: a TPR study with H_2 and CO as reducing agents. Journal of Catalysis, 225, 267-277.
25. Damyanova, S., Pawelec, B., Arishtirova, K., Huerta, M. M., and Fierro, G.J.L. (2008) Study of the surface and redox properties of ceria-zirconia oxides. Applied Catalysis A: General, 337, 86-96.

Table 4.1 Specific surface area, pore size, and pore volume of MSP $Ce_{0.75}Zr_{0.25}O_2$ at different stirring times via the nanocasting process

Stirring time	BET Surface area (m^2/g)	Pore size (nm)*	Pore volume (cm^3/g)
30 min	205.4 ± 5.7	1.42 ± 0.08	0.31 ± 0.01
1 h	237.6 ± 6.2	4.31 ± 0.02	0.40 ± 0.01
2 h	243.1 ± 6.7	3.81 ± 0.02	0.48 ± 0.05
4 h	248.5 ± 8.8	3.39 ± 0.02	0.43 ± 0.01

Table 4.2 Specific surface area, pore size, and pore volume of MSP $Ce_{0.75}Zr_{0.25}O_2$ at different evaporated temperatures via the nanocasting process

(Evaporated temperature)	BET Surface area (m^2/g)	Pore size (nm)	Pore volume (cm^3/g)
RT.	233.3 ± 13.9	3.83 ± 0.50	0.29 ± 0.13
50 °C	214.9 ± 5.2	3.82 ± 0.02	0.32 ± 0.04
100 °C	248.5 ± 8.8	3.39 ± 0.02	0.43 ± 0.01

Table 4.3 XRF analysis of the order MSP ceria-zirconia

Sample	Ce (%)	Zr (%)	Si (%)
$Ce_{0.60}Zr_{0.40}O_2$	81.27	18.73	3.68
$Ce_{0.75}Zr_{0.25}O_2$	88.08	11.92	2.88

Table 4.4 Specific surface area, pore size, and pore volume of the synthesis order MSP $Ce_{1-x}Zr_xO_2$ via the nanocasting process

Ce : Zr ratio	**BET Surface area (m^2/g)**	**Pore size (nm)**	**Pore volume (cm^3/g)**
75 : 25	248.5 ± 8.8	3.39 ± 0.02	0.43 ± 0.01
60 : 40	205.7 ± 16.6	1.39 ± 0.01	0.38 ± 0.05

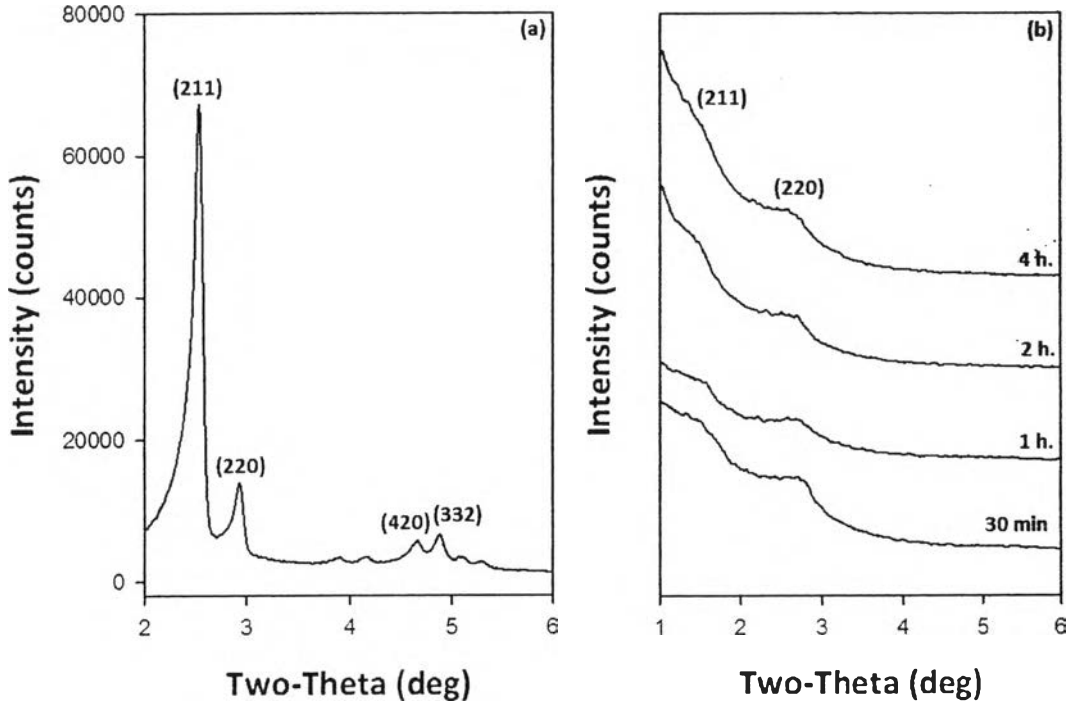

Figure 4.1 Small angle XRD patterns of a) MCM-48 and b) $Ce_{0.75}Zr_{0.25}O_2$ at various stirring times via the nanocasting process.

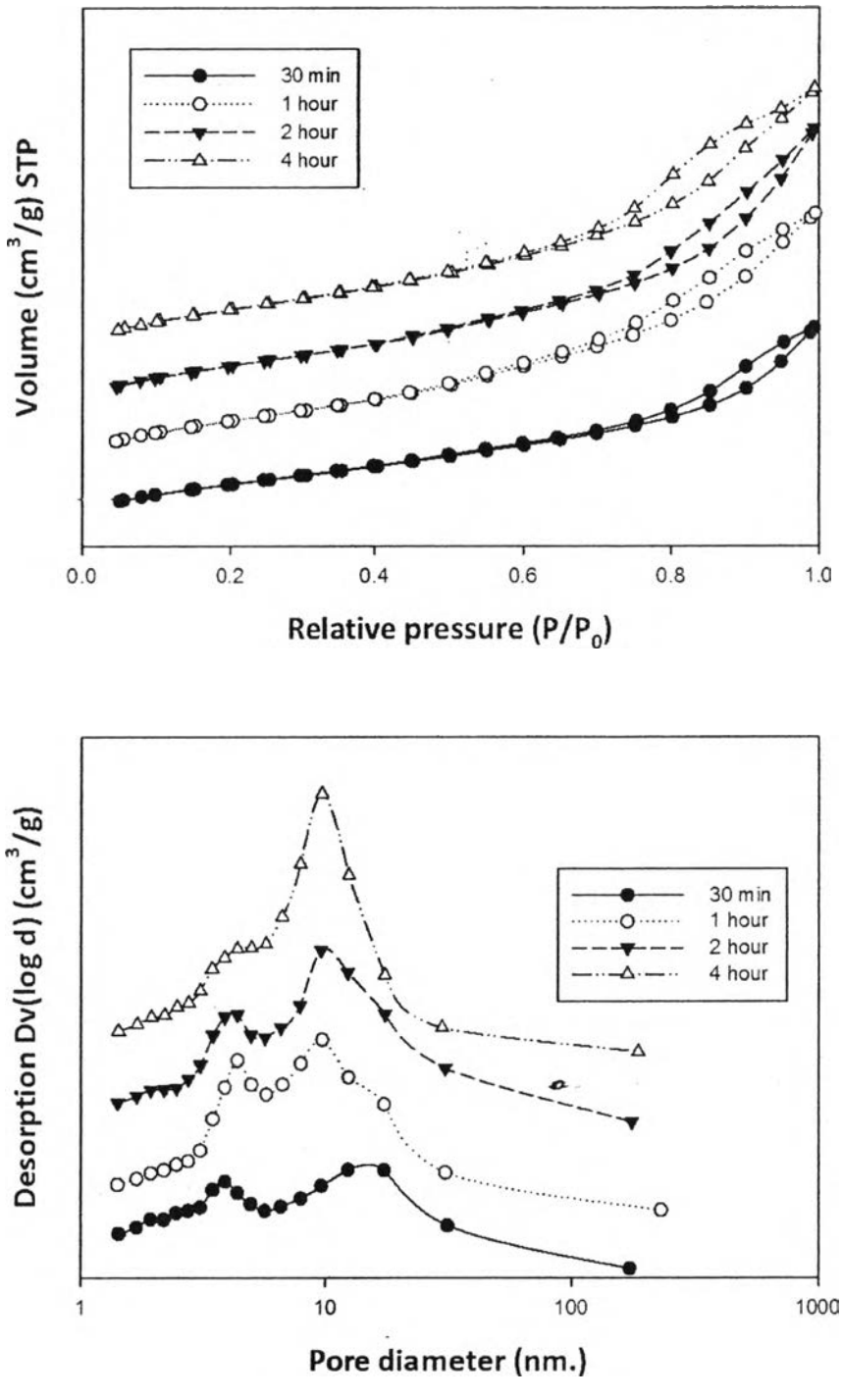

Figure 4.2 (a) N_2 adsorption-desorption isotherm and (b) pore size distribution of the ordered MSP $Ce_{0.75}Zr_{0.25}O_2$ resulted from various stirring times.

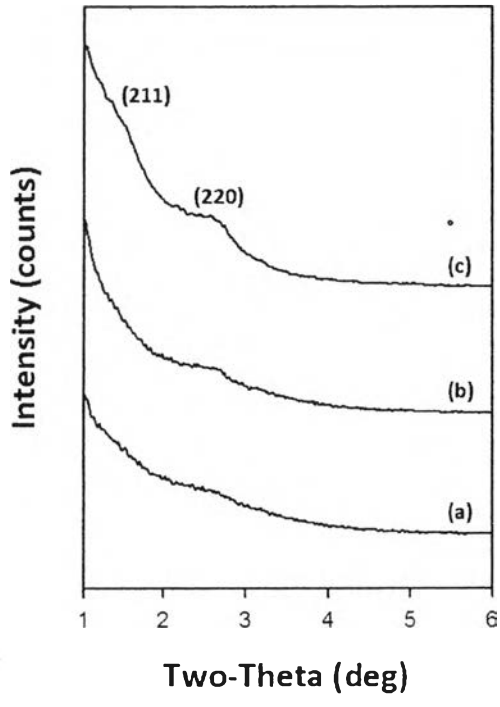

Figure 4.3 Small angle XRD patterns of MSP $Ce_{0.75}Zr_{0.25}O_2$ at a) ambient temperature; b) 50 °, and c) 100 °C evaporated temperature via the nanocasting process.

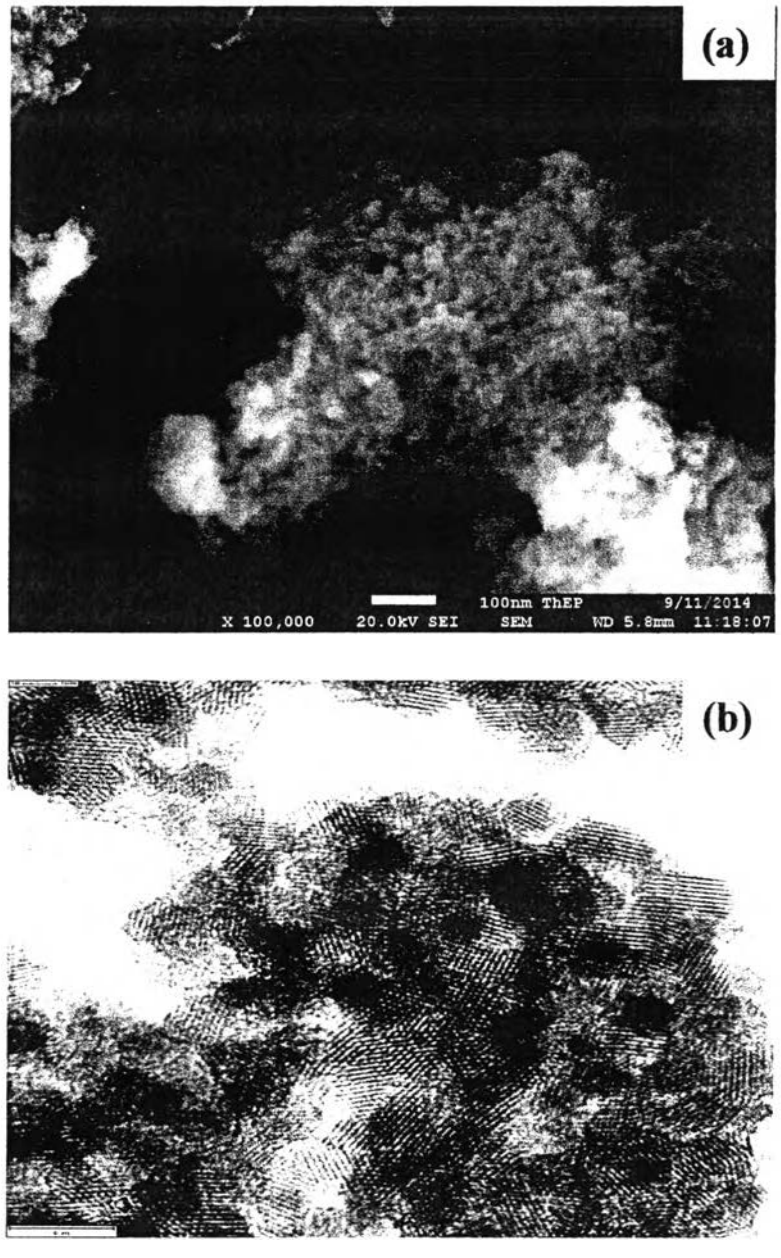

Figure 4.4 a) SEM and b) TEM images of the synthesized ordered MSP $Ce_{0.75}Zr_{0.25}O_2$.

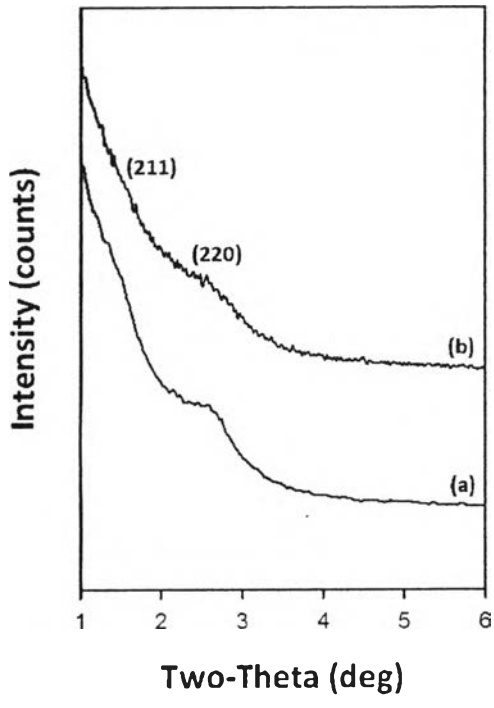

Figure 4.5 Small angle XRD patterns of a) $Ce_{0.75}Zr_{0.25}O_2$, and b) $Ce_{0.60}Zr_{0.40}O_2$.

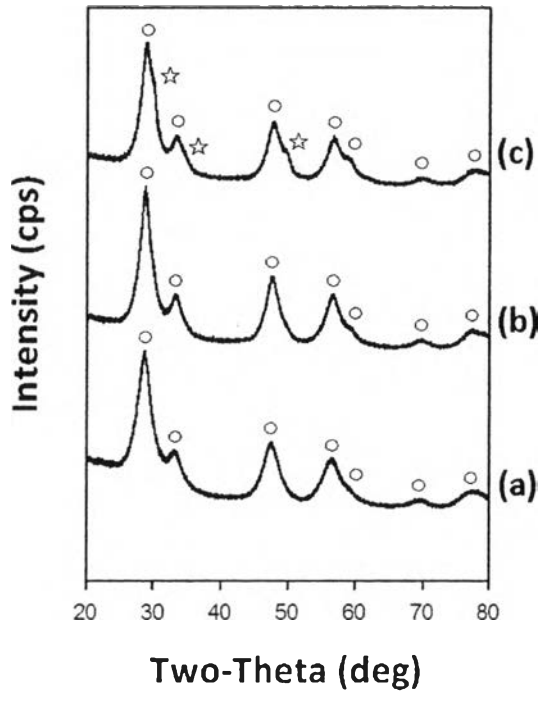

Figure 4.6 Wide angle XRD patterns of a) CeO_2; b.) $Ce_{0.75}Zr_{0.25}O_2$, and c) $Ce_{0.75}Zr_{0.25}O_2$ by (○) cubic phase, and (☆) tetragonal phase.

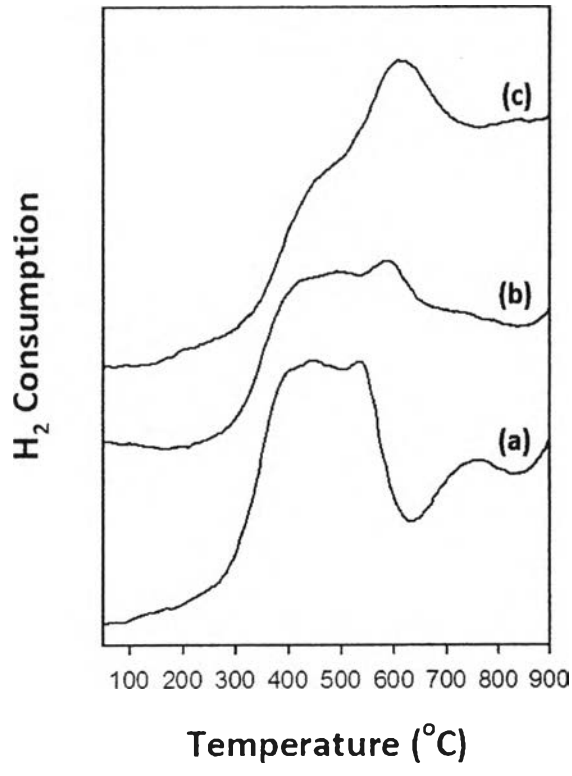

Figure 4.7 TPR profiles of order MSP a) CeO_2, b) $Ce_{0.75}Zr_{0.25}O_2$, and c) $Ce_{0.60}Zr_{0.40}O_2$.